Chapter 12

Genetically Engineering a Susceptible Mouse Model for MERS-CoV-Induced Acute Respiratory Distress Syndrome

Sarah R. Leist and Adam S. Cockrell

Abstract

Since 2012, monthly cases of Middle East respiratory syndrome coronavirus (MERS-CoV) continue to cause severe respiratory disease that is fatal in ~35% of diagnosed individuals. The ongoing threat to global public health and the need for novel therapeutic countermeasures have driven the development of animal models that can reproducibly replicate the pathology associated with MERS-CoV in human infections. The inability of MERS-CoV to replicate in the respiratory tracts of mice, hamsters, and ferrets stymied initial attempts to generate small animal models. Identification of human dipeptidyl peptidase IV (hDPP4) as the receptor for MERS-CoV infection *opened the door* for genetic engineering of mice. Precise molecular engineering of mouse DPP4 (mDPP4) with clustered regularly interspaced short palindromic repeats (CRISPR)/Cas9 technology maintained inherent expression profiles, and limited MERS-CoV susceptibility to tissues that naturally express mDPP4, notably the lower respiratory tract wherein MERS-CoV elicits severe pulmonary pathology. Here, we describe the generation of the 288–330$^{+/+}$ MERS-CoV mouse model in which mice were made susceptible to MERS-CoV by modifying two amino acids on mDPP4 (A288 and T330), and the use of adaptive evolution to generate novel MERS-CoV isolates that cause fatal respiratory disease. The 288–330$^{+/+}$ mice are currently being used to evaluate novel drug, antibody, and vaccine therapeutic countermeasures for MERS-CoV. The chapter starts with a historical perspective on the emergence of MERS-CoV and animal models evaluated for MERS-CoV pathogenesis, and then outlines the development of the 288–330$^{+/+}$ mouse model, assays for assessing a MERS-CoV pulmonary infection in a mouse model, and describes some of the challenges associated with using genetically engineered mice.

Key words Middle East respiratory syndrome coronavirus, Mouse, Clustered regularly interspaced short palindromic repeats, Cas9, Pathogenesis

1 Introduction

In February of 2018 MERS-CoV was listed as a priority on the R&D Blueprint for the global strategy and preparedness plan outlined by the World Health Organization (WHO) [1]. The R&D Blueprint includes viruses that pose a global public health risk, and for which there are no available therapeutic countermeasures [1]. Twenty-seven countries have reported cases of MERS-CoV

Rahul Vijay (ed.), *MERS Coronavirus: Methods and Protocols*, Methods in Molecular Biology, vol. 2099,
https://doi.org/10.1007/978-1-0716-0211-9_12,

with most cases confined to the Arabian Peninsula. Diagnosed cases of MERS-CoV in countries outside the Arabian Peninsula are primarily traveler associated. The potential for global spread of MERS-CoV was realized in 2015 when a single traveler returning to South Korea initiated an outbreak that infected 186 people resulting in 20% fatality and caused widespread fear that crippled the economy for nearly 6 months [2–4]. Human-to-human transmission is often associated with close contact in the health care setting, but can also occur between family members within a household [5]. Asymptomatic individuals pose a particular risk of transmission due to their unknown carrier status as demonstrated in the health care setting [6]. Despite the high percent of fatalities associated with MERS-CoV outbreaks on the Arabian Peninsula most epidemiological studies suggest R_0 values <1, indicative of a low risk of sustainable human-to-human transmission, whereas epidemiological studies from the South Korean outbreak describe R_0 values (>1) akin to more sustainable human-to-human transmission [7]. Recurring spillover events from dromedary camels (zoonotic reservoir for MERS-CoV on the Arabian Peninsula) likely contribute to newly diagnosed cases in humans [8–10]. The potential for continuous reintroduction to humans increases the risk of MERS-CoV adapting in humans to acquire enhanced human-to-human transmission profiles, a scenario suspected to have initiated the SARS-CoV pandemic in 2002–2003 [11]. Effective public health measures and culling of civet cats, the zoonotic host for SARS-CoV, brought the SARS-CoV pandemic to a rapid end [11]. Eliminating MERS-CoV through culling of infected camel herds is not a practical solution. Furthermore, detection of pre-emergent MERS-CoV-like, and SARS-CoV-like, strains circulating in bat species indicate that the natural environment is ripe for future human exposures to potentially pathogenic coronaviruses [12–14]. Therefore, the development of therapeutic countermeasures that can interfere with MERS-CoV pathogenesis is critical to break zoonotic-to-human and human-to-human transmission cycles that may instigate global spread.

Evaluating the toxicity and efficacy of novel MERS-CoV therapeutics require the availability of animal models that effectively recapitulate MERS-CoV pathogenesis during fatal cases of human infections. Therefore, the first question in generating a MERS-CoV animal model would be: What are the pathological features of a human infection? Limited histopathological findings from human autopsies indicate that fatal cases of MERS-CoV results from pneumonia initiated by infection of bronchiolar and alveolar epithelia of the lower respiratory tract (LRT) [15, 16]. Pneumonia in the LRT is also the prominent finding on radiographs from X-rays and CTs of diagnosed human cases [17]. High viral loads in tracheal aspirates from patients are also associated with severe pulmonary disease [18], which is indicative of actively replicating MERS-CoV in the LRT. Initial evaluation of the human MERS-CoV EMC/2012

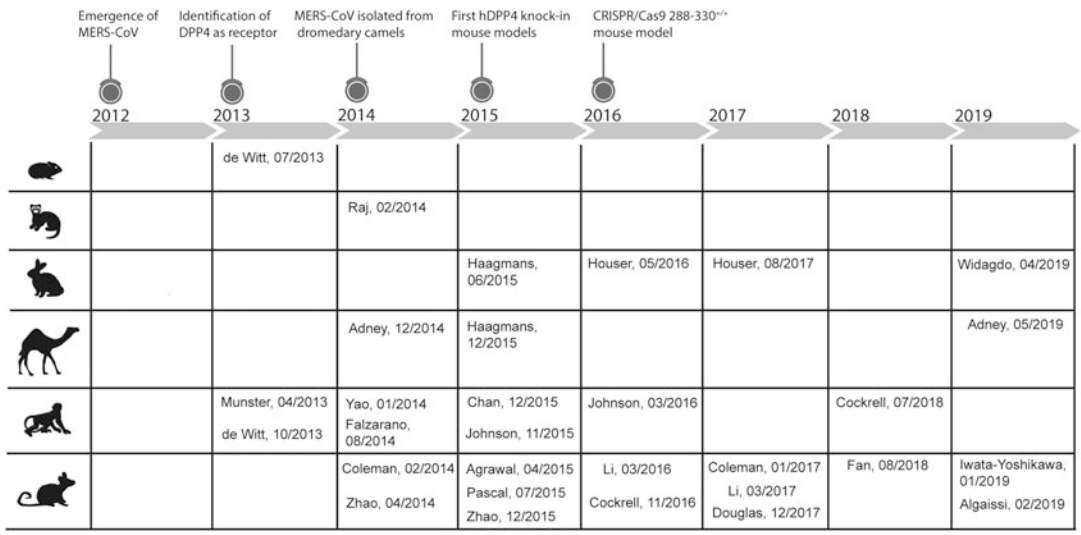

Fig. 1 Timeline of the mammalian models evaluated for MERS-CoV pathogenesis between 2012 and 2019. Specific events since the emergence of MERS-CoV in 2012 are emphasized above the timeline. References to mammalian models evaluated for MERS-CoV pathogenesis comprise hamster [19], ferret [20], rabbit [21–24], camel [25–27], nonhuman primates [28–35], and mouse [36–48]

isolate in rhesus macaques demonstrated replication in the LRT with mild pneumonia-like disease (Fig. 1) [28]. Achieving respiratory pathology reflecting a lethal human disease proved to be more complicated in nonhuman primates. Severe respiratory disease in the marmoset produced clinical endpoints consistent with fatal disease that required euthanasia (Fig. 1) [29, 30]. Evaluation of two human isolates, Jordan and EMC/2012, and a tissue culture-adapted MERS-CoV strain (MERS-0) in nonhuman primates resulted in mild disease in rhesus macaques or marmosets (Fig. 1) [31–33], confounding the reproducibility of near-lethal disease in NHPs. Nonhuman primates are central to late-stage preclinical evaluation of therapeutic countermeasures, but may be impractical for initial preclinical studies. A small animal model may be applicable if there is limited therapeutic available for toxicity and efficacy testing, especially if large animal numbers are needed to determine confidence and reproducibility.

Early studies in mouse, hamster, and ferret revealed that conventional small animal models were fully resistant to MERS-CoV infection and replication (Fig. 1) [19, 20, 36]. A seminal study identifying the MERS-CoV receptor as human dipeptidyl peptidase IV (hDPP4) [49], and publication of the crystal structure of hDPP4 interacting with the receptor binding domain (RBD) of the MERS-CoV spike protein [50], exposed tropism determinants critical for susceptibility. Dipeptidyl peptidase IV contact amino acids at the hDPP4/RBD interface are highly conserved among MERS-CoV-susceptible mammalian species (human, camel, and

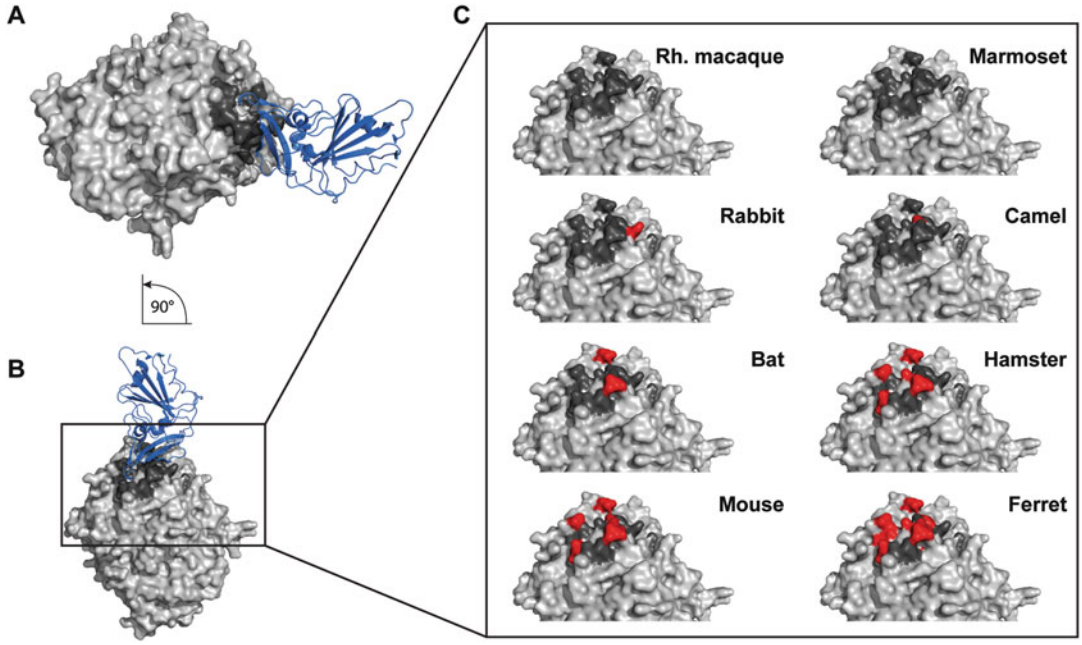

Fig. 2 Comparison of DPP4 from different species. (**a**) Horizontal view of the crystal structure (PDB, 4L72) of human DPP4 (light gray) interacting with the MERS-CoV receptor binding domain (RBD; blue). The contact residues of human DPP4 with MERS-CoV RBD are highlighted in dark gray. (**b**) A 90° rotation, demonstrating the vertical view of (A). (**c**) Zoomed-in view of the human DPP4 structure (light gray) with highlighted MERS-CoV RBD contact residues (dark gray). Species-specific contact residues that differ from human are highlighted in red

bat) (Fig. 2) [51]. Although mouse, hamster, ferret, and guinea pig DPP4 orthologs exhibit high overall similarity to hDPP4, specific amino acid differences at the DPP4/RBD interface account for the inability of these species to support infection [51–56]. Overexpression of a mouse DPP4 (mDPP4) with changes in the contact residues at the DPP4/RBD altered cellular profiles from resistant to susceptible to MERS-CoV infection [52, 53, 56]. The dependence on DPP4-specific contact was further substantiated by similar studies evaluating modified DPP4 orthologs from the hamster, ferret, and guinea pig [55]. Dipeptidyl peptidase IV was identified as the major determinant of MERS-CoV tropism.

1.1 MERS-CoV Mouse Models

Researchers rapidly leveraged knowledge of the DPP4 receptor to generate susceptible small animal models (Fig. 1) [12]. Zhao et al. utilized a unique approach for producing susceptible mice that could replicate human isolates of MERS-CoV in the lungs by infecting mouse lungs with an adenovirus that constitutively expresses the full-length hDPP4 gene (Fig. 1) [37]. Transient expression of hDPP4 supported infection and replication with human strains of MERS-CoV in the lungs and indicated that this technology may be an effective rapid response platform for initial

evaluation of emergent and pre-emergent viruses. However, pathology associated with a fatal MERS-CoV infection was not observed in the Ad-hDPP4 model [37], which limited the capacity to evaluate the efficacy of therapeutic countermeasures.

Genetic engineering of mice would be necessary to develop preclinical MERS-CoV mouse models with respiratory phenotypes that reflected clinical outcomes in patients. Knock-in of full-length hDPP4 rendered mice susceptible to human isolates of MERS-CoV at low infection doses (Fig. 1) [38–40]. Knock-in mice exhibited severe pulmonary pathology and increased mortality; however, widespread constitutive expression of full-length hDPP4 resulted in high levels of MERS-CoV infection and replication in extrapulmonary tissues [38–40]. In some studies, higher viral loads could be detected in the brain compared to the lungs [39, 40]. Mice with infections of the central nervous system (CNS) exhibited encephalitis that corresponded with the kinetics of mortality [39]. Currently, there is no evidence to support a CNS component associated with MERS-CoV pathogenesis in humans. Attempts to restrict hDPP4 expression to epithelial cells of the lungs using constitutive tissue specific promoters (e.g., cytokeratin K18) yielded outcomes similar to those observed with SARS-CoV mouse models, wherein high levels of MERS-CoV infection/replication were detected in the brains (Fig. 1) [39].

To circumvent confounding problems associated with global bio-distribution of overexpressed hDPP4 receptor, researchers engineered mouse models using sophisticated molecular approaches. Pascal et al. employed Regeneron's VelociGene technology to replace sequences encoding nearly the entire mDPP4 genomic region with those encoding the exons/introns from the hDPP4 genetic region (Fig. 1) [41]. Retaining the mDPP4 5′ and 3′ genetic elements that regulate expression maintained inherent expression profiles of full-length hDPP4 in mice [41]. Importantly, MERS-CoV infection/replication was readily detected in the lungs with little involvement of extrapulmonary tissues [41]. Infection with human isolates of MERS-CoV caused moderate respiratory pathology with mortality determined by euthanasia of mice at 20% weight loss [41]. Unfortunately, commercial restrictions limit the availability and use of this model to the broader scientific community. In addition to the concerns raised above, the first generation of mouse models was developed with the full-length hDPP4, which may alter the inherent physiological properties of the mouse.

The multifaceted involvement of DPP4 in maintaining immune homeostasis is of significant importance regarding susceptibility to infectious disease [57]. DPP4 exists in two forms: (1) a membrane anchored form on the surface of multiple cells types (e.g., B cells, T cells, NK cells, and epithelial cells to mention a few) and (2) a secreted form that can be identified in human serum [57]. DPP4 interacts with and modifies heterologous protein molecules

involved in nociception, neuroendocrine function, metabolism, cardiovascular function, immune regulation, and infection [57]. Modification of heterologous protein function can proceed through cleavage of *N*-terminal amino acids through the enzymatic activity of the α/*b*-hydroxylase domain, or allosteric interaction/signal transduction [57]. The species specificity of DPP4 is exemplified by the interaction of hDPP4 with adenosine deaminase (ADA), a well-recognized binding partner of hDPP4, which modulates downstream T cell functions [58–60]. The hDPP4/ADA interaction evolved in higher mammalian species (human, NHP, bovine, rabbit), but not in mouse or rat [58–60]. Interestingly, in one study ADA was demonstrated to block infection of MERS-CoV in tissue culture [20], indicating that the binding site on hDPP4 for ADA, and the MERS-CoV RBD, may overlap. Consequently, introducing full-length hDPP4 into mice may skew innate immune mechanisms that could influence responses to therapeutic countermeasures.

In the second generation of MERS-CoV-susceptible mouse models amino acid residues predicted to function at the mDPP4/MERS-CoV RBD interface were modified to avoid the introduction of full-length hDPP4 (Fig. 1) [42, 43]. Li et al. recently developed a mouse model wherein the *mDPP4* genomic region encompassing exons 10–12 were replaced with the respective genomic region from *hDPP4*, referred to as an hDPP4 knock-in model (hDPP4-KI) [43]. Exons 10–12 encode contact amino acids at the hDPP4/MERS-CoV RBD interface that were able to support replication of human MERS-CoV isolates in the lungs, but did not elicit a mortality phenotype [43]. Adaptive evolution of human MERS-CoV in the hDPP4-KI mouse resulted in mouse-adapted viruses that evoked a lethal respiratory phenotype with little involvement of extrapulmonary tissues. The lethal respiratory phenotype is a consequence of novel mutations acquired during adaptive evolution. A combination of mutations in both the S1 and S2 regions of the MERS-CoV spike protein facilitated a lethal respiratory phenotype [43]. Results in the hDPP4-KI model substantiate an earlier mouse model referred to as the 288–330$^{+/+}$ model, which was designed with only two amino acid changes in mDPP4 to generate MERS-CoV susceptible mice.

Genetic engineering and implementation of the 288–330$^{+/+}$ mouse model, combined with MERS-CoV adaptive evolution, is the subject of this chapter. Initial studies in tissue culture revealed that human and rodent cell types were resistant to MERS-CoV infection upon overexpression of mDPP4; however, overexpression of hDPP4 conferred permissivity to infection/replication [53]. Comparative structural modeling of hDPP4 and mDPP4 revealed putative contact residues in mDPP4 amenable to modification at the DPP4/RBD interface. Modification of two amino acids (A288L and T330R) was sufficient to endow mDPP4 with

the capacity to mediate MERS-CoV infection/replication [53]. Shortly after the emergence of MERS-CoV into humans in 2012, the CRISPR/Cas9 genome editing technology became available for applications to modify mammalian genomes in vitro and in vivo [61–63]. Recognizing our unique situation, we designed CRISPR/Cas9 targets to modify the mouse genome encoding amino acids A288 and T330 in exons 10 and 11 of the *mDPP4* gene (Fig. 3) [12, 42]. Concomitant with mouse development, in vitro studies were initiated to adapt MERS-CoV to the modified mDPP4 [42]. Tissue culture adaption resulted in MERS-0 virus, which contained an RMR insertion and S885L mutation in the S2 region of the MERS-CoV spike protein [42]. A MERS-0 molecular clone exhibited enhanced replication kinetics and higher titers compared to human MERS-CoV isolates. Additionally, the MERS-0 virus replicated to higher levels in the lungs of 288–330$^{+/+}$ mice, compared to human and camel MERS-CoV isolates [42]. Based on these data the MERS-0 virus was used to initiate passaging in mice heterozygous for mDPP4 with A288L and T330R mutations, 288–330$^{+/-}$ (Fig. 4). We reasoned that adaptation around one expressed copy of the mDPP4 with 288–330 mutations, and a wild-type mDPP4 expressed copy, might cultivate generation of a mouse-adapted MERS-CoV that could utilize wild-type mDPP4 as the primary receptor. After 15 passages we obtained a mouse-adapted MERS-CoV (MERS15c2) exhibiting a lethal respiratory phenotype in the 288–330$^{+/+}$ mice [42]. Our MERS-CoV reverse genetic system was used to generate an infectious clone of the mouse-adapted virus, icMERSma1 [42]. Lethal respiratory pathology with icMERSma1 required high infectious doses (5×10^6 Pfu). An additional 20 passages of icMERSma1 in 288–330$^{+/-}$ mice bore a novel mouse-adapted MERS-CoV that produced lethal respiratory disease at doses of 5×10^5 Pfu, and lung pathology associated with severe respiratory disease at 5×10^4 to 5×10^5 Pfu [44] (Fig. 1). This MERS-CoV model system (288–330$^{+/+}$ mice and mouse-adapted MERS-CoV viruses) is now being employed to: (1) understand complex virus-host interactions [12, 31, 42, 64–67], (2) evaluate antibody-based therapeutics [42], (3) evaluate drug-based therapeutic countermeasures [68], and (4) evaluate anti-MERS-CoV vaccines [42, 66]. The goal of this chapter is to provide an outline of how to rationally design a mouse with altered susceptibility to MERS-CoV. For additional information there are a number of detailed reviews and book chapters describing the design and utilization of the CRISPR/Cas9 technology for generating mouse models [69, 70].

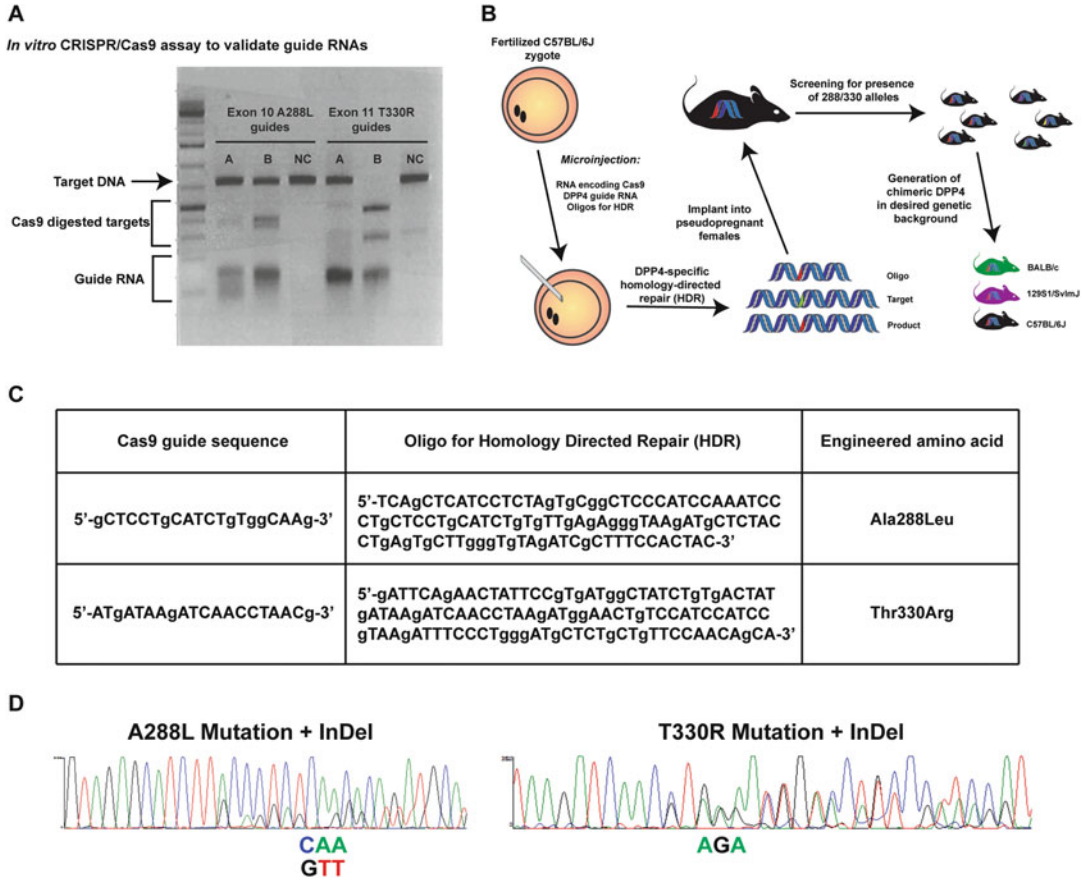

Fig. 3 CRISPR/Cas9 mediated genetic engineering of mouse DPP4. (**a**) In vitro validation of guide RNAs via Cas9 endonuclease assay (image was kindly provided by Dale Cowley in the Animal Models Core Facility at the University of North Carolina). Agarose gel separation based on size allows for discrimination between target DNA, Cas9 digested targets, and guide RNAs. (**b**) Schematic utilizing CRISPR/Cas9 technology to genetically engineer mice. Fertilized C57BL/6 J zygotes are collected and injected with RNA encoding Cas9, DPP4 single guide RNA, and oligos to facilitate homology-directed repair (HDR). Microinjected zygotes are implanted into pseudopregnant recipient female C57BL/6 J mice. Offspring are screened by sequencing for the intended change at positions 288 and 330. Mice identified as having the appropriate changes are backcrossed to C57BL/6 J mice to maintain the pure C57BL/6 J background, or may be crossed to any desired strain (e.g., BALB/cJ or 129S1/SvImJ). (**c**) Table describing sequences of Cas9 guide RNAs and oligos for HDR to genetically engineer amino acid changes at position 288 (Ala to Leu) and 330 (Thr to Arg). (**d**) Sequencing chromatograms highlighting how the F0 offspring from embryo implantation can be a mosaic of insertion/deletions (InDel's) generated by random non-homologous end joining from Cas9 cutting at the genomic alleles, and the HDR repair that incorporates the intended changes encoding amino acids at positions 288 and 330. Pure homozygous 288–330$^{+/+}$ lines were obtained by backcrossing onto C57BL/6 J mice. The highlighted mutations CAA (TTG in the reverse orientation) and AGA encode the novel 288 L and 330R amino acids

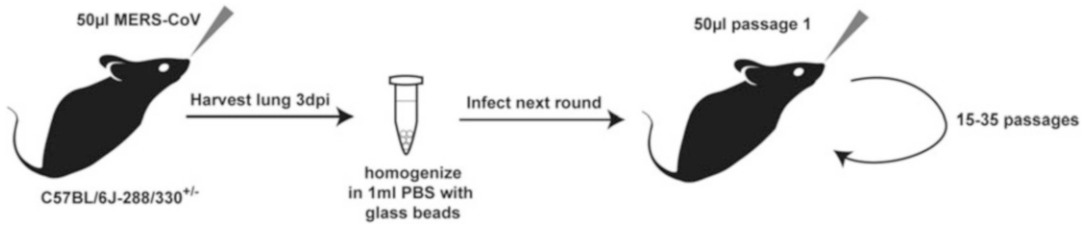

Fig. 4 Mouse adaptation of MERS-0 in 288–330$^{+/-}$ mice. 288/330$^{+/-}$ mice were intranasally infected with 50 µL of MERS-0. Three days after infection lungs were harvested, homogenized in 1 mL PBS with glass beads, and 50 µL of the supernatant from the lung homogenate was used to infect the next round of 288–330$^{+/-}$ mice. Serial lung passages are performed for 15 [42] to 35 [44] rounds

2 Materials

2.1 Tissue Culture Adaptation of MERS-CoV to mDPP4 Harboring the A288L and T330R Mutations

1. Mouse fibroblast NIH/3T3 cells (ATCC, cat# CRL-1658) stably expressing mDPP4 with A288L and T330R mutations [42].
2. NIH/3T3 maintenance in standard DMEM media supplemented with 10% FBS and 1× antibiotic/antimycotic.
3. MERS-CoV-tRFP recombinant virus generated using coronavirus reverse genetics [71].
4. See plaque assay materials for clonal isolation and expansion (Subheading 2.8).

2.2 Intranasal Infection of 288–330$^{+/+}$ Mice

1. Virus diluted in viral growth medium (OptiMEM, 3% Fetal Clone II, 1× antibiotic/antimycotic, 1× NEAA). Select a virus concentration that is appropriate for the specific study design.
2. Sterile 1 mL syringes and needles.
3. Ketamine/xylazine mixture (100 mg/mL stock solution, Akorn, Lake Forest, IL).
4. Scale capable of weighing mice ranging from 10 to 50 g.
5. Ear punch tool.

2.3 Monitoring Morbidity and Mortality

1. Scale capable of weighing mice ranging from 10 to 50 g.
2. Plastic cup to hold mice while weighing.
3. Plastic square to cover plastic cup.

2.4 Assessment of Respiratory Function as Additional Metric for Morbidity

1. Buxco system.

2.5 Harvest of Lungs from Infected Mice

1. Scale capable of weighing mice ranging from 10 to 50 g.
2. Sealable jar filled with paper towels and isoflurane (99.9% isofluorane, Piramal, Andhra Pradesh, India).
3. Styrofoam board.
4. Two 50 mL conical tubes filled with 70% ethanol and Cidecon.
5. Scissors, forceps, and metal pins.
6. Collection tubes prefilled with appropriate solutions.

2.6 Harvest of Bronchoalveolar Lavage (BAL) from Infected Mice

1. Styrofoam board.
2. Sealable jar filled with paper towels and isoflurane.
3. Two 50 mL conical tubes filled with 70% ethanol and Cidecon.
4. Surgical tools (scissors, forceps, and metal pins).
5. Collection tubes.
6. Safelet catheters 22G X1″(Exel International).
7. PBS filled 1 mL luer lock syringe.

2.7 Harvest of Blood and BAL for Hematological Analysis via VetScan HM5

1. Styrofoam board.
2. Sealable jar filled with paper towels and isoflurane.
3. Two 50 mL conical tubes filled with 70% ethanol and Cidecon.
4. Surgical tools (scissors, forceps, and metal pins).
5. EDTA prefilled collection tubes.
6. Safelet catheters.
7. PBS filled 1 mL luer lock syringe.

2.8 Plaque Assay of Lungs from Infected Mice

1. Homogenizer.
2. Centrifuge.
3. Vero CCL81 cells (ATCC, Manassas, VA) grown in appropriate medium (DMEM, 10% Fetal Clone II, 1× antibiotic/antimycotic).
4. 6-Well plates.
5. Two bottles (250 mL or 500 mL) for overlay.
6. Dilution tube boxes (96 tube format) filled with 450 μL PBS.
7. Overlay: one bottle with water and agarose (0.8 g/100 mL); one bottle with 2× medium (high glucose MEM, 20% Fetal Clone II, 2× antibiotic/antimycotic).
8. Microwave.
9. Bead bath (37 °C and 56 °C).
10. Incubator at 37 °C.

3 Methods

Important: All experiments using MERS-CoV strains should be executed under BSL3 conditions in accordance with Institutional Biosafety Committee approval, and under the governance of the National Institute of Allergy and Infectious Diseases within the National Institute of Health.

3.1 Tissue Culture Adaptation of MERS-CoV to mDPP4 Harboring the A288L and T330R Mutations (See Note 1)

1. Passaging was initiated with a MERS-CoV infectious clone generated using reverse genetics techniques to staple together sequences similar to the human EMC/2012 strain [71, 72] (*see* **Note 2**).
2. Mouse NIH 3T3 cells were generated to stably express the mDPP4 containing the A288L and T330R mutations [42] (*see* **Note 3**).
3. Seed NIH 3T3 cells stably expressing the modified mDPP4 receptor on 6-well plates at 1×10^6 cells/well.
4. 24 h after seeding, infect cells with the rMERS-CoV at an MOI of 0.1–0.001 (*see* **Note 4**).
5. If the virus is labeled with a fluorescent marker, cells are monitored for increased fluorescence at 24, 48, and 72 h post-infection using a fluorescent microscope (*see* **Note 5**).
6. Plaque-like islands of tRFP-expressing cells are indicative of replicating virus.
7. Harvest supernatant from infected cells at 48 to72 h. This is considered the passage 1 (P1) virus.
8. The passaging cycle is continued by diluting the supernatant 1:100–1:1000 and repeating the infection on fresh NIH/3T3 cells stably expressing mDPP4 with the A288L and T330R mutations.
9. After a predetermined number of passages the region encoding the spike protein of MERS-CoV is sequenced using RT-PCR to amplify the region of interest followed by standard Sanger sequencing (*see* **Note 6**).
10. After 10 passages viruses were plaque purified by diluting the heterogenous stock of virus $10^{-1}$to 10^{-6}, and infecting a monolayer of Vero CCL81 cells similar to a standard plaque assay.
11. Single plaques are isolated using a pipet tip and the virus expanded on a freshly seeded monolayer of Vero CCL81 cells.
12. Virus stocks are generated, viral RNA is isolated using standard TRIzol purification, and the region encoding the MERS-CoV spike protein is amplified by standard RT-PCR techniques and sequenced using standard Sanger sequencing.

13. Mutations identified by sequencing must be confirmed using a reverse genetic system to generate an infectious clone encoding the identified mutations [72]. Cockrell et al. validated the MERS-0 virus in this manner [42].

3.2 Engineering the 288–330$^{+/+}$ Mouse Model with CRISPR/Cas9 Homology-Directed Repair Genome Editing (Fig. 3)

The details for generating and using the CRISPR/Cas9 system to generate mutations are outlined in the materials and methods by Cockrell et al. [42]. Notably, the 288–330$^{+/+}$ mice were initially generated in the Animal Models Core facility at the University of North Carolina at Chapel Hill. The extensive technical expertise required for genetic engineering of mice is the subject of many expert reviews and book chapters that will not be covered here. Nevertheless, we provide a conceptual overview of the steps to generate the 288–330$^{+/+}$ mice.

1. Design guide RNAs to target each of the A288 and T330 alleles. Cockrell et al. designed the guide RNAs to direct the Cas9 to cut as near the mutation site as possible (Fig. 3) (*see* **Note 7** for helpful resources to design and genetically engineer mouse knockouts).
2. Test guide RNAs in vitro for the capacity to cut a target sequence (Fig. 3).
   (a) Generate double-stranded ODNs or a plasmid containing the target sequence with the correct PAM site.
   (b) Assemble ribonucleoprotein (RNP) complexes according to manufacturer's instructions (*see* **Note 8**).
   (c) Subject double-stranded DNA with target sequence to RNP complexes and assess digestion pattern on an agarose gel (Fig. 3).
3. Two separate oligos are also designed to introduce the novel mutations on exons 10 (A288L) and 11 (T330R) of mDPP4, through homology-directed repair (Fig. 3).
4. Fertilized zygotes are collected from C57BL/6J female mice that were superovulated and mated to male C57BL/6J mice.
5. In vitro transcribed RNAs encoding the guide sequences and Cas9 endonuclease, combined with ODNs encoding the replacement alleles for 288 and 330 in mDPP4, were all pronuclear injected into the fertilized zygote [42] (Fig. 3). The fertilized zygotes were from C57BL/6J mice.
6. The injected embryos were implanted into pseudopregnant recipient females.
7. Newly born pups were screened for the presence of the correct change at the 288 and 330 alleles by standard PCR amplification and Sanger sequencing (Fig. 3) (*see* **Note 9**).

8. Mice identified to have both mutations were crossed with wild-type C57BL/6J mice to obtain heterozygous mice with the mutated 288 L and 330R alleles in *cis*.
9. The F1 heterozygous mice were intercrossed to generate homozygous breeders to develop the 288–330$^{+/+}$ colony, and for utilization in subsequent experiments.
10. The mouse colony is maintained under conditions delineated by the institutional Department of Comparative Medicine (DCM) and Institutional Animal Use and Care Committee (IACUC).

Important: All experiments infecting mice with various MERS-CoV wild-type or recombinant isolates are performed under BSL3/ABSL3 conditions. The generation of recombinant isolates requires prior approval of the Institutional Biosafety Committee (IBC). Additionally, all animal experiments should have prior approval according to the Institutional Animal Use and Care Committee (IACUC), Institutional Biosafety Committee (IBC), and in accordance with the recommendations for the care and use of animals by the Office of Laboratory Animal Welfare at NIH.

3.3 Intranasal Infection of 288–330$^{+/-}$ and 288–330$^{+/+}$ Mice

1. Mice are randomly assigned into cohorts specifically paying attention to include age- and sex-matched control animals.
2. Individual mice are made identifiable (e.g., ear notch, ear clip, tail mark).
3. 288–330$^{+/+}$ mice are brought into the BSL3 laboratory 7 days before start of the experiment to allow for environmental acclimation.
4. Mice are anesthetized via intraperitoneal injection of 50–100 μL of a ketamine (50 mg/kg)/xylazine (15 mg/kg) mixture (*see* **Note 10**).
5. Level of anesthesia is assessed by pedal reflex.
6. Measure initial weight (Day 0 weight) while waiting for mouse to be anesthetized (*see* **Note 11**).
7. Once a pedal reflex is no longer triggered, mice should be immediately infected by the intranasal route. Holding the animal vertically, apply 50 μL of virus solution by pipetting onto their nostrils and allow them to inhale. To ensure that all of the 50 μL reach the lower respiratory tract hold the mouse upright for an additional 30 s (*see* **Note 12**).
8. Note any inconsistencies during infection, including: (1) presence of bubbles of inoculum from nasal cavity, (2) occurrence of inoculum in mouth, or (3) failure to inhale entire dose of inoculum. Notes will help to explain potential inconsistencies in readout parameters and may be used as exclusion criteria for inefficient infections.

9. Mice are put back into the cage and placed on their back to ensure virus solution will stay in the lungs. Note: Cages are returned to cage rack, but the respiration of mice is continuously monitored by observing breathing.
10. Place mice next to each other to keep body temperature as close to normal as possible.
11. Check cage after 30–45 min to confirm that all mice wake up from anesthesia and infection.

3.4 Mouse Adaptation of MERS-0 in 288–330$^{+/-}$ Mice (Fig. 4)

1. Mouse adaptation was initiated in heterozygous 288–330$^{+/-}$ mice by infecting with 50 μL of the MERS-0 infectious clone (*see* **Note 13**).
2. At 3 days post-infection the mouse is euthanized by extended exposure to isoflurane. ~2 mL of isoflurane is added to the bottom of a jar that can be firmly sealed (*see* **Note 14**).
3. A thoracotomy is performed to expose the lungs.
4. Lungs are removed and placed in a 2 mL gasket sealed skirted screw cap tubes. Tubes are previously prepared with 1 mL of 1× PBS containing ~5–10 mm of glass beads.
5. Lungs are homogenized for 60 s in a bead homogenizer.
6. Lung lysates are centrifuged in a microcentrifuge for 5 min at max speed to pellet debris.
7. This is considered passage 1 (P1) and 50 μL of lung homogenate is used to infect a naïve 288–330$^{+/-}$ mouse.
8. The process is repeated for a desired number of cycles.

3.5 Monitoring Morbidity and Mortality

1. After infection mice are monitored daily for weight loss for the entire duration of the experiment.
2. To record daily weights, pick up mice by the tail, identify by ear notch, and place into cup on a scale. Record weight and calculate percentage of starting body weight (*see* **Note 15**).
3. Mice can also be monitored to determine if they are moribund using a clinical scoring scale whereby: 0 = no clinical signs; 1 = ruffled fur; 2 = ruffled fur with hunched posture (only slight with no signs of dehydration); 3 = as defined in number 2 with more severe signs of dehydration and some loss of body strength; 4 = pronounced dehydration and prominent loss of mobility; 5 = unresponsive to stimuli and prominent eye squinting.
4. It is important to note that weight loss might not always be the most appropriate parameter and animals should be euthanized at the discretion of the researcher even if animals have not reached 80% of their starting weight.

5. Mice that approach 80% of their starting body weight (20% weight loss) are euthanized via isoflurane overdose followed by a secondary euthanasia method (thoracotomy or cervical dislocation). Depending on the experimental circumstances an institutionally approved exception may be implemented to allow continuation of the experiment (increasing the frequency with which the mice are monitored will likely need to be implemented) (*see* **Note 16**).

3.6 Assessment of Respiratory Function as an Additional Metric for Morbidity (A Brief Stepwise Overview)

1. Acclimate individual mice for 30 min in plethysmography chamber (Buxco System, Wilmington, NC). A study by Menachery et al. comprehensively describes the application of plethysmography to infectious respiratory viruses in mouse models [73] (*see* **Note 17**).
2. A variety of lung function-related parameters are then recorded over a period of 5 min [e.g., enhanced pause (PenH), mid-tidal expiratory flow (EF50), peak expiratory flow (PEF), and peak inspiratory flow (PIF)].
3. Respiratory function can be performed every day over the entire course of infection, or on single selected days. Investigating a novel respiratory virus may require the investigator to perform a time course to determine the most effective time points for measurement. The largest differences between groups typically correlate with peak viral replication.
4. At each time point measured the mice need to be randomized into different chambers to avoid technical artifacts (e.g., a mouse measured at day 1 in chamber 1 should be evaluated in a different chamber on day 2 measurement). Practical considerations dictate that 8–12 animals can be measured at any one time, and each group of 8–12 mice may take an hour for a proficient technician. Therefore, experiments should be carefully planned to limit the number of mice to be evaluated.
5. Mice that are difficult to handle can be slightly anesthetized by applying isoflurane to the chamber in order to remove them from the chamber and return to their cage (*see* **Note 18**).

3.7 Measuring Lung Hemorrhage for Gross Assessment of Pathology and Harvesting the Lungs

Important: Removal of all samples from BSL3 facilities must be executed in accordance with the Institutional Biosafety Committee. Assays must either be performed inside the BSL3 laboratory or additional processing steps (validated to fully inactivate virus and approved by the IBC) must be executed before removal of samples to a BSL2 setting.

1. Sacrifice mice by isoflurane overdose.
2. Place on scale and record endpoint weights.

3. Pin mouse on all four extremities to Styrofoam board using metal pins.
4. Spray with 70% ethanol to avoid contamination of samples with fur.
5. Remove fur over thorax.
6. Open thorax, paying attention not to cut into lung tissue.
7. Assess lung tissue for reddish discoloration and record severity by applying a number 0 (no hemorrhaging) to 4 (severe hemorrhaging in all lobes of the lungs).
8. Harvest lung tissue and place in tubes prefilled with sample type specific solution.
9. Put scissors and forceps first into Cidecon to remove any residual blood and then into 70% ethanol in order to not cross-contaminate samples.
10. Whole lung can be used for one assay or different lobes can be used for different assays.

3.8 Collecting Blood from Infected Mice

1. **Steps 1–6** from Subheading 3.7.
2. Cut into superior vena cava and collect blood with a pipette.
3. Blood is typically transferred to a serum/plasma separation tube that allows for separation of serum/plasma from cells.
4. In the event that it is necessary to harvest cells for flow cytometry analysis or VetScan HM5 analysis, the blood sample can be transferred to a tube containing EDTA. Note: VetScan HM5 is a veterinary diagnostic machine that analyzes basic immune cell counts and additional hematological parameters within 2 min.
5. All VetScan assays are performed under BSL3 conditions. Removal of samples for downstream analysis outside of BSL3 conditions require specific inactivation procedures that must be pre-approved by the institutional biosafety committee.

3.9 Collecting Bronchoalveolar Lavage (BAL) from Infected Mice

1. **Steps 1–6** from Subheading 3.7.
2. Expose trachea and enter with catheter.
3. Remove needle part of catheter and attach 1 ml luer lock syringe prefilled with 1 mL of 1× PBS.
4. Carefully inject 1 mL PBS into lungs, wait for 30 s, and pull 1× PBS back out. This is the BAL sample.
5. Place sample into a fresh collection tube.
6. Use a new catheter for every mouse.
7. In the event that it is necessary to harvest cells for flow cytometry analysis or VetScan HM5 analysis, the BAL sample can

be transferred to an empty tube or a tube containing EDTA, respectively.

8. All VetScan assays are performed under BSL3 conditions. Removal of samples for downstream analysis outside of BSL3 conditions require specific inactivation procedures that must be pre-approved by the institutional biosafety committee.

3.10 Plaque Assay of Lungs from Infected Mice (Performed Under BSL3 Conditions)

1. One day prior to performing the assay, seed 5×10^5 Vero CCL81 cells into each well of a 6-well plate (one plate per sample).
2. Prepare overlay: 2× medium + agar in water (1:1). You will need 2 mL overlay per well.
3. Place 2× medium bottle into 37 °C bead bath.
4. Heat 0.8% agar in water in a microwave and place at 56 °C.
5. Thaw lung samples in tubes filled with 1 mL of 1× PBS and glass beads.
6. Once thawed, place into tissue homogenizer for 60 s.
7. Centrifuge at 13,000 rpm (~15,000 × g) for 5 min.
8. Transfer 50 μL of sample into 450 μL of PBS. Mix samples well.
9. Perform serial tenfold dilutions (10^{-1} to 10^{-6}).
10. Transfer 200 μL of each dilution to individual wells on a 6-well plate.
11. Incubate for 1 h, rocking 6-well plates every 15 min.
12. Mix 2× medium with dissolved agarose.
13. Put 2 mL of overlay onto every well.
14. Place in 37 °C incubator for 3 days.
15. Virus plaques are visualized by neutral red staining (2 mL/well) and using a lightbox. Count plaques to determine the number of plaque forming units per milliliter (Pfu/mL).

4 Notes

1. It is not necessary to initiate MERS-CoV adaptation in tissue culture first, as was demonstrated by Li et al. [43]. Nonetheless, Cockrell et al. chose to initiate their MERS-CoV adaptation studies on tissue culture cells while the 288–330$^{+/+}$ mice were in the process of being generated [42]. Therefore, for the purposes of this chapter this is included as a potential starting point for MERS-CoV adaptation.
2. Cockrell et al. initiated adaptation experiments with a rMERS-CoV expressing the tomato red protein in place of the Orf5 ORF [42, 71, 72].

3. This can also be achieved using a readily transfectable human embryonic fibroblast cell line such as HEK293T cells and selecting for stably transfected cells.
4. Cells can be counted by seeding an extra well, but it is safe to assume that the cell number is approximately doubled after 24 h.
5. This can also be achieved using a microscope to assess plaque size if plaques can be readily detected.
6. Since the major determinant of MERS-CoV tropism is the spike protein, it would be anticipated that mutations having the most significant impact on infection might occur within the gene encoding the spike protein. Nonetheless, as described by Cockrell et al., Douglas et al., and Li et al., a number of mouse-adapted mutations were identified in genetic regions outside of the spike gene, which may have a significant influence on virus fidelity and evasion of host immune responses [42–44].
7. At the time that these mice were being generated in early 2014, CRISPR/Cas9 reagents were not readily available. Additionally, there were few bioinformatics tools available to facilitate guide RNA design and off-target potential. In the current research environment CRISPR/Cas9 reagents can be sourced from multiple commercial entities and there are a number of bioinformatics tools to assist with design. Addgene is a non-profit plasmid repository where CRISPR reagents and resources can be readily obtained (https://www.addgene.org/). Additional guidance for generating mice using CRISPR/Cas9 technology can be found in more comprehensive protocols [69, 70].
8. All relevant reagents and protocols can now be obtained from commercial sources as readily synthesized RNAs and purified proteins (e.g., Integrated DNA Technologies).
9. Although a number of pups may be identified to have the correct mutation, many will likely be mosaic for random mutations including insertions/deletions due to the higher efficiency of non-homologous end joining (NHEJ) after Cas9 digestion compared to the desired HDR employed to mediate allele modification.
10. The administered dose will depend on the weight of the animal which should be predetermined the day prior to initiating the experiment.
11. It is not necessary to anesthetize mice for measuring daily weights.
12. It is important that the inoculum reaches the lower respiratory tract for a successful MERS-CoV infection.
13. Mouse adaptation can be initiated with any MERS-CoV strain that exhibits some pulmonary replication.

14. Mice should never come into contact with the isoflurane. To prevent direct contact, a layer of aluminum foil is placed at the bottom of the jar and this is covered with two additional layers of paper towel.
15. The percent body weight is typically calculated after leaving the BSL3 environment. Therefore, the weight sheets should have the anticipated weights of each animal at 20% weight loss. This will provide a real-time indication of when the mice are approaching the criteria established for humane euthanasia.
16. Institutional approval is required for animals to be placed under exception. It cannot be emphasized enough that all animal work should be pre-approved by appropriate University IACUC and IBC committees and should be in accordance with the recommendations for the care and use of animals by the Office of Laboratory Animal Welfare at NIH.
17. Assessing respiratory function using plethysmography under BSL3 conditions requires costly equipment and extensive training prior to use.
18. Anesthesia should be avoided prior to measuring lung function to prevent interference with lung function measurements.

References

1. Mehand MS, Al-Shorbaji F, Millett P, Murgue B (2018) The WHO R&D Blueprint: 2018 review of emerging infectious diseases requiring urgent research and development efforts. Antivir Res 159:63–67
2. Bernard-Stoecklin S, Nikolay B, Assiri A, Bin Saeed AA, Ben Embarek PK, El Bushra H, Ki M, Malik MR, Fontanet A, Cauchemez S, Van Kerkhove MD (2019) Comparative analysis of eleven healthcare-associated outbreaks of Middle East respiratory syndrome coronavirus (Mers-Cov) from 2015 to 2017. Sci Rep 9:7385
3. Joo H, Maskery BA, Berro AD, Rotz LD, Lee YK, Brown CM (2019) Economic impact of the 2015 MERS outbreak on the Republic of Korea's tourism-related industries. Health Secur 17:100–108
4. Lee SI (2015) Costly lessons from the 2015 Middle East respiratory syndrome coronavirus outbreak in Korea. J Prev Med Public Health 48:274–276
5. Hui DS, Azhar EI, Kim Y-J, Memish ZA, M-d O, Zumla A (2018) Middle East respiratory syndrome coronavirus: risk factors and determinants of primary, household, and nosocomial transmission. Lancet Infect Dis 18: e217–e227
6. Alfaraj SH, Al-Tawfiq JA, Altuwaijri TA, Alanazi M, Alzahrani N, Memish ZA (2018) Middle East respiratory syndrome coronavirus transmission among health care workers: implication for infection control. Am J Infect Control 46:165–168
7. Park JE, Jung S, Kim A, Park JE (2018) MERS transmission and risk factors: a systematic review. BMC Public Health 18:574
8. Alshukairi AN, Zheng J, Zhao J, Nehdi A, Baharoon SA, Layqah L, Bokhari A, Al Johani SM, Samman N, Boudjelal M, Ten Eyck P, Al-Mozaini MA, Zhao J, Perlman S, Alagaili AN (2018) High prevalence of MERS-CoV infection in camel workers in Saudi Arabia. MBio 9
9. Conzade R, Grant R, Malik MR, Elkholy A, Elhakim M, Samhouri D, Ben Embarek PK, Van Kerkhove MD (2018) Reported direct and indirect contact with dromedary camels among laboratory-confirmed MERS-CoV cases. Viruses 10:E425
10. Hemida MG, Elmoslemany A, Al-Hizab F, Alnaeem A, Almathen F, Faye B, Chu DK, Perera RA, Peiris M (2017) Dromedary camels and the transmission of Middle East respiratory syndrome coronavirus (MERS-CoV). Transbound Emerg Dis 64:344–353

11. Peiris JS, Guan Y, Yuen KY (2004) Severe acute respiratory syndrome. Nat Med 10:S88–S97
12. Cockrell AS, Leist SR, Douglas MG, Baric RS (2018) Modeling pathogenesis of emergent and pre-emergent human coronaviruses in mice. Mamm Genome 29:367–383
13. Cui J, Li F, Shi ZL (2019) Origin and evolution of pathogenic coronaviruses. Nat Rev Microbiol 17:181–192
14. Menachery VD, Graham RL, Baric RS (2017) Jumping species-a mechanism for coronavirus persistence and survival. Curr Opin Virol 23:1–7
15. Alsaad KO, Hajeer AH, Al Balwi M, Al Moaiqel M, Al Oudah N, Al Ajlan A, AlJohani S, Alsolamy S, Gmati GE, Balkhy H, Al-Jahdali HH, Baharoon SA, Arabi YM (2018) Histopathology of Middle East respiratory syndrome coronovirus (MERS-CoV) infection—clinicopathological and ultrastructural study. Histopathology 72:516–524. https://doi.org/10.1111/his.13379
16. Ng DL, Al Hosani F, Keating MK, Gerber SI, Jones TL, Metcalfe MG, Tong S, Tao Y, Alami NN, Haynes LM, Mutei MA, Abdel-Wareth L, Uyeki TM, Swerdlow DL, Barakat M, Zaki SR (2016) Clinicopathologic, immunohistochemical, and ultrastructural findings of a fatal case of Middle East respiratory syndrome coronavirus infection in the United Arab Emirates, April 2014. Am J Pathol 186:652–658
17. Arabi YM, Balkhy HH, Hayden FG, Bouchama A, Luke T, Baillie JK, Al-Omari A, Hajeer AH, Senga M, Denison MR, Nguyen-Van-Tam JS, Shindo N, Bermingham A, Chappell JD, Van Kerkhove MD, Fowler RA (2017) Middle East respiratory syndrome. N Engl J Med 376:584–594
18. Oh MD, Park WB, Choe PG, Choi SJ, Kim JI, Chae J, Park SS, Kim EC, Oh HS, Kim EJ, Nam EY, Na SH, Kim DK, Lee SM, Song KH, Bang JH, Kim ES, Kim HB, Park SW, Kim NJ (2016) Viral load kinetics of MERS coronavirus infection. N Engl J Med 375:1303–1305
19. de Wit E, Prescott J, Baseler L, Bushmaker T, Thomas T, Lackemeyer MG, Martellaro C, Milne-Price S, Haddock E, Haagmans BL, Feldmann H, Munster VJ (2013) The Middle East respiratory syndrome coronavirus (MERS-CoV) does not replicate in Syrian hamsters. PLoS One 8:e69127
20. Raj VS, Smits SL, Provacia LB, van den Brand JM, Wiersma L, Ouwendijk WJ, Bestebroer TM, Spronken MI, van Amerongen G, Rottier PJ, Fouchier RA, Bosch BJ, Osterhaus AD, Haagmans BL (2014) Adenosine deaminase acts as a natural antagonist for dipeptidyl peptidase 4-mediated entry of the Middle East respiratory syndrome coronavirus. J Virol 88:1834–1838
21. Haagmans BL, van den Brand JM, Provacia LB, Raj VS, Stittelaar KJ, Getu S, de Waal L, Bestebroer TM, van Amerongen G, Verjans GM, Fouchier RA, Smits SL, Kuiken T, Osterhaus AD (2015) Asymptomatic Middle East respiratory syndrome coronavirus infection in rabbits. J Virol 89:6131–6135
22. Houser KV, Broadbent AJ, Gretebeck L, Vogel L, Lamirande EW, Sutton T, Bock KW, Minai M, Orandle M, Moore IN, Subbarao K (2017) Enhanced inflammation in New Zealand white rabbits when MERS-CoV reinfection occurs in the absence of neutralizing antibody. PLoS Pathog 13:e1006565
23. Houser KV, Gretebeck L, Ying T, Wang Y, Vogel L, Lamirande EW, Bock KW, Moore IN, Dimitrov DS, Subbarao K (2016) Prophylaxis with a Middle East respiratory syndrome coronavirus (MERS-CoV)-specific human monoclonal antibody protects rabbits from MERS-CoV infection. J Infect Dis 213:1557–1561
24. Widagdo W, Okba NMA, Richard M, de Meulder D, Bestebroer TM, Lexmond P, Farag E, Al-Hajri M, Stittelaar KJ, de Waal L, van Amerongen G, van den Brand JMA, Haagmans BL, Herfst S (2019) Lack of Middle East respiratory syndrome coronavirus transmission in rabbits. Viruses 11:E381
25. Adney DR, Letko M, Ragan IK, Scott D, van Doremalen N, Bowen RA, Munster VJ (2019) Bactrian camels shed large quantities of Middle East respiratory syndrome coronavirus (MERS-CoV) after experimental infection. Emerg Microbes Infect 8:717–723
26. Adney DR, van Doremalen N, Brown VR, Bushmaker T, Scott D, de Wit E, Bowen RA, Munster VJ (2014) Replication and shedding of MERS-CoV in upper respiratory tract of inoculated dromedary camels. Emerg Infect Dis 20:1999–2005
27. Haagmans BL, van den Brand JM, Raj VS, Volz A, Wohlsein P, Smits SL, Schipper D, Bestebroer TM, Okba N, Fux R, Bensaid A, Solanes Foz D, Kuiken T, Baumgartner W, Segales J, Sutter G, Osterhaus AD (2016) An orthopoxvirus-based vaccine reduces virus excretion after MERS-CoV infection in dromedary camels. Science 351:77–81
28. Munster VJ, de Wit E, Feldmann H (2013) Pneumonia from human coronavirus in a macaque model. N Engl J Med 368:1560–1562
29. Chan JF, Yao Y, Yeung ML, Deng W, Bao L, Jia L, Li F, Xiao C, Gao H, Yu P, Cai JP, Chu H,

Zhou J, Chen H, Qin C, Yuen KY (2015) Treatment with lopinavir/ritonavir or interferon-beta1b improves outcome of MERS-CoV infection in a nonhuman primate model of common marmoset. J Infect Dis 212:1904–1913

30. Falzarano D, de Wit E, Feldmann F, Rasmussen AL, Okumura A, Peng X, Thomas MJ, van Doremalen N, Haddock E, Nagy L, LaCasse R, Liu T, Zhu J, McLellan JS, Scott DP, Katze MG, Feldmann H, Munster VJ (2014) Infection with MERS-CoV causes lethal pneumonia in the common marmoset. PLoS Pathog 10: e1004250
31. Cockrell AS, Johnson JC, Moore IN, Liu DX, Bock KW, Douglas MG, Graham RL, Solomon J, Torzewski L, Bartos C, Hart R, Baric RS, Johnson RF (2018) A spike-modified Middle East respiratory syndrome coronavirus (MERS-CoV) infectious clone elicits mild respiratory disease in infected rhesus macaques. Sci Rep 8:10727
32. Johnson RF, Bagci U, Keith L, Tang X, Mollura DJ, Zeitlin L, Qin J, Huzella L, Bartos CJ, Bohorova N, Bohorov O, Goodman C, Kim DH, Paulty MH, Velasco J, Whaley KJ, Johnson JC, Pettitt J, Ork BL, Solomon J, Oberlander N, Zhu Q, Sun J, Holbrook MR, Olinger GG, Baric RS, Hensley LE, Jahrling PB, Marasco WA (2016) 3B11-N, a monoclonal antibody against MERS-CoV, reduces lung pathology in rhesus monkeys following intratracheal inoculation of MERS-CoV Jordan-n3/2012. Virology 490:49–58
33. Johnson RF, Via LE, Kumar MR, Cornish JP, Yellayi S, Huzella L, Postnikova E, Oberlander N, Bartos C, Ork BL, Mazur S, Allan C, Holbrook MR, Solomon J, Johnson JC, Pickel J, Hensley LE, Jahrling PB (2015) Intratracheal exposure of common marmosets to MERS-CoV Jordan-n3/2012 or MERS-CoV EMC/2012 isolates does not result in lethal disease. Virology 485:422–430
34. de Wit E, Rasmussen AL, Falzarano D, Bushmaker T, Feldmann F, Brining DL, Fischer ER, Martellaro C, Okumura A, Chang J, Scott D, Benecke AG, Katze MG, Feldmann H, Munster VJ (2013) Middle East respiratory syndrome coronavirus (MERS-CoV) causes transient lower respiratory tract infection in rhesus macaques. Proc Natl Acad Sci U S A 110:16598–16603
35. Yao Y, Bao L, Deng W, Xu L, Li F, Lv Q, Yu P, Chen T, Xu Y, Zhu H, Yuan J, Gu S, Wei Q, Chen H, Yuen KY, Qin C (2014) An animal model of MERS produced by infection of rhesus macaques with MERS coronavirus. J Infect Dis 209:236–242
36. Coleman CM, Matthews KL, Goicochea L, Frieman MB (2014) Wild-type and innate immune-deficient mice are not susceptible to the Middle East respiratory syndrome coronavirus. J Gen Virol 95:408–412
37. Zhao J, Li K, Wohlford-Lenane C, Agnihothram SS, Fett C, Zhao J, Gale MJ Jr, Baric RS, Enjuanes L, Gallagher T, McCray PB Jr, Perlman S (2014) Rapid generation of a mouse model for Middle East respiratory syndrome. Proc Natl Acad Sci U S A 111:4970–4975
38. Agrawal AS, Garron T, Tao X, Peng BH, Wakamiya M, Chan TS, Couch RB, Tseng CT (2015) Generation of a transgenic mouse model of Middle East respiratory syndrome coronavirus infection and disease. J Virol 89:3659–3670
39. Li K, Wohlford-Lenane C, Perlman S, Zhao J, Jewell AK, Reznikov LR, Gibson-Corley KN, Meyerholz DK, McCray PB Jr (2016) Middle East Respiratory syndrome coronavirus causes multiple organ damage and lethal disease in mice transgenic for human dipeptidyl peptidase 4. J Infect Dis 213:712–722
40. Zhao G, Jiang Y, Qiu H, Gao T, Zeng Y, Guo Y, Yu H, Li J, Kou Z, Du L, Tan W, Jiang S, Sun S, Zhou Y (2015) Multi-organ damage in human dipeptidyl peptidase 4 transgenic mice infected with Middle East respiratory syndrome-coronavirus. PLoS One 10: e0145561
41. Pascal KE, Coleman CM, Mujica AO, Kamat V, Badithe A, Fairhurst J, Hunt C, Strein J, Berrebi A, Sisk JM, Matthews KL, Babb R, Chen G, Lai KM, Huang TT, Olson W, Yancopoulos GD, Stahl N, Frieman MB, Kyratsous CA (2015) Pre- and postexposure efficacy of fully human antibodies against Spike protein in a novel humanized mouse model of MERS-CoV infection. Proc Natl Acad Sci U S A 112:8738–8743
42. Cockrell AS, Yount BL, Scobey T, Jensen K, Douglas M, Beall A, Tang XC, Marasco WA, Heise MT, Baric RS (2016) A mouse model for MERS coronavirus-induced acute respiratory distress syndrome. Nat Microbiol 2:16226
43. Li K, Wohlford-Lenane CL, Channappanavar R, Park JE, Earnest JT, Bair TB, Bates AM, Brogden KA, Flaherty HA, Gallagher T, Meyerholz DK, Perlman S, McCray PB Jr (2017) Mouse-adapted MERS coronavirus causes lethal lung disease in human DPP4 knockin mice. Proc Natl Acad Sci U S A 114:E3119–E3128
44. Douglas MG, Kocher JF, Scobey T, Baric RS, Cockrell AS (2018) Adaptive evolution influences the infectious dose of MERS-CoV

necessary to achieve severe respiratory disease. Virology 517:98–107

45. Algaissi A, Agrawal AS, Han S, Peng BH, Luo C, Li F, Chan TS, Couch RB, Tseng CK (2019) Elevated human dipeptidyl peptidase 4 expression reduces the susceptibility of hDPP4 transgenic mice to Middle East respiratory syndrome coronavirus infection and disease. J Infect Dis 219:829–835
46. Coleman CM, Sisk JM, Halasz G, Zhong J, Beck SE, Matthews KL, Venkataraman T, Rajagopalan S, Kyratsous CA, Frieman MB (2017) CD8+ T cells and macrophages regulate pathogenesis in a mouse model of Middle East respiratory syndrome. J Virol 91:e01825
47. Fan C, Wu X, Liu Q, Li Q, Liu S, Lu J, Yang Y, Cao Y, Huang W, Liang C, Ying T, Jiang S, Wang Y (2018) A human DPP4-Knockin Mouse's susceptibility to infection by authentic and pseudotyped MERS-CoV. Viruses 10: E448
48. Iwata-Yoshikawa N, Okamura T, Shimizu Y, Kotani O, Sato H, Sekimukai H, Fukushi S, Suzuki T, Sato Y, Takeda M, Tashiro M, Hasegawa H, Nagata N (2019) Acute respiratory infection in human dipeptidyl peptidase 4-transgenic mice infected with Middle East respiratory syndrome coronavirus. J Virol 93: e01818
49. Raj VS, Mou H, Smits SL, Dekkers DH, Muller MA, Dijkman R, Muth D, Demmers JA, Zaki A, Fouchier RA, Thiel V, Drosten C, Rottier PJ, Osterhaus AD, Bosch BJ, Haagmans BL (2013) Dipeptidyl peptidase 4 is a functional receptor for the emerging human coronavirus-EMC. Nature 495:251–254
50. Wang N, Shi X, Jiang L, Zhang S, Wang D, Tong P, Guo D, Fu L, Cui Y, Liu X, Arledge KC, Chen YH, Zhang L, Wang X (2013) Structure of MERS-CoV spike receptor-binding domain complexed with human receptor DPP4. Cell Res 23:986–993
51. Peck KM, Burch CL, Heise MT, Baric RS (2015) Coronavirus host range expansion and Middle East respiratory syndrome coronavirus emergence: biochemical mechanisms and evolutionary perspectives. Annu Rev Virol 2:95–117
52. Barlan A, Zhao J, Sarkar MK, Li K, McCray PB Jr, Perlman S, Gallagher T (2014) Receptor variation and susceptibility to Middle East respiratory syndrome coronavirus infection. J Virol 88:4953–4961
53. Cockrell AS, Peck KM, Yount BL, Agnihothram SS, Scobey T, Curnes NR, Baric RS, Heise MT (2014) Mouse dipeptidyl peptidase 4 is not a functional receptor for Middle East respiratory syndrome coronavirus infection. J Virol 88:5195–5199
54. Peck KM, Cockrell AS, Yount BL, Scobey T, Baric RS, Heise MT (2015) Glycosylation of mouse DPP4 plays a role in inhibiting Middle East respiratory syndrome coronavirus infection. J Virol 89:4696–4699
55. Peck KM, Scobey T, Swanstrom J, Jensen KL, Burch CL, Baric RS, Heise MT (2017) Permissivity of dipeptidyl peptidase 4 orthologs to Middle East respiratory syndrome coronavirus is governed by glycosylation and other complex determinants. J Virol 91:e00534
56. van Doremalen N, Miazgowicz KL, Milne-Price S, Bushmaker T, Robertson S, Scott D, Kinne J, McLellan JS, Zhu J, Munster VJ (2014) Host species restriction of Middle East respiratory syndrome coronavirus through its receptor, dipeptidyl peptidase 4. J Virol 88:9220–9232
57. Klemann C, Wagner L, Stephan M, von Horsten S (2016) Cut to the chase: a review of CD26/dipeptidyl peptidase-4's (DPP4) entanglement in the immune system. Clin Exp Immunol 185:1–21
58. Kameoka J, Tanaka T, Nojima Y, Schlossman SF, Morimoto C (1993) Direct association of adenosine deaminase with a T cell activation antigen, CD26. Science 261:466–469
59. Ohnuma K, Dang NH, Morimoto C (2008) Revisiting an old acquaintance: CD26 and its molecular mechanisms in T cell function. Trends Immunol 29:295–301
60. Weihofen WA, Liu J, Reutter W, Saenger W, Fan H (2004) Crystal structure of CD26/dipeptidyl-peptidase IV in complex with adenosine deaminase reveals a highly amphiphilic interface. J Biol Chem 279:43330–43335
61. Cong L, Ran FA, Cox D, Lin S, Barretto R, Habib N, Hsu PD, Wu X, Jiang W, Marraffini LA, Zhang F (2013) Multiplex genome engineering using CRISPR/Cas systems. Science 339:819–823
62. Mali P, Yang L, Esvelt KM, Aach J, Guell M, DiCarlo JE, Norville JE, Church GM (2013) RNA-guided human genome engineering via Cas9. Science 339:823–826
63. Yang H, Wang H, Shivalila CS, Cheng AW, Shi L, Jaenisch R (2013) One-step generation of mice carrying reporter and conditional alleles by CRISPR/Cas-mediated genome engineering. Cell 154:1370–1379
64. Chefer S, Seidel J, Cockrell AS, Yount B, Solomon J, Hagen KR, Liu DX, Huzella LM, Kumar MR, Postnikova E, Bohannon JK, Lackemeyer MG, Cooper K, Endlich-Frazier A, Sharma H, Thomasson D, Bartos C, Sayre PJ,

Sims A, Dyall J, Holbrook MR, Jahrling PB, Baric RS, Johnson RF (2018) The human sodium iodide symporter as a reporter gene for studying Middle East respiratory syndrome coronavirus pathogenesis. mSphere 3:e00540

65. Leist SR, Baric RS (2018) Giving the genes a shuffle: using natural variation to understand host genetic contributions to viral infections. Trends Genet 34:777–789
66. Menachery VD, Gralinski LE, Mitchell HD, Dinnon KH 3rd, Leist SR, Yount BL Jr, Graham RL, McAnarney ET, Stratton KG, Cockrell AS, Debbink K, Sims AC, Waters KM, Baric RS (2017) Middle East respiratory syndrome coronavirus nonstructural protein 16 is necessary for interferon resistance and viral pathogenesis. mSphere 2:e00346
67. Menachery VD, Mitchell HD, Cockrell AS, Gralinski LE, Yount BL Jr, Graham RL, McAnarney ET, Douglas MG, Scobey T, Beall A, Dinnon K 3rd, Kocher JF, Hale AE, Stratton KG, Waters KM, Baric RS (2017) MERS-CoV accessory ORFs play key role for infection and pathogenesis. MBio 8:e00665
68. Sheahan TP, Sims AC, Graham RL, Menachery VD, Gralinski LE, Case JB, Leist SR, Pyrc K, Feng JY, Trantcheva I, Bannister R, Park Y, Babusis D, Clarke MO, Mackman RL, Spahn JE, Palmiotti CA, Siegel D, Ray AS, Cihlar T, Jordan R, Denison MR, Baric RS (2017) Broad-spectrum antiviral GS-5734 inhibits both epidemic and zoonotic coronaviruses. Sci Transl Med 9:eaal3653
69. Huijbers IJ (2017) Generating genetically modified mice: a decision guide. Methods Mol Biol 1642:1–19
70. Scott GJ, Gruzdev A (2019) Genome editing in mouse embryos with CRISPR/Cas9. Methods Mol Biol 1960:23–40
71. Scobey T, Yount BL, Sims AC, Donaldson EF, Agnihothram SS, Menachery VD, Graham RL, Swanstrom J, Bove PF, Kim JD, Grego S, Randell SH, Baric RS (2013) Reverse genetics with a full-length infectious cDNA of the Middle East respiratory syndrome coronavirus. Proc Natl Acad Sci U S A 110:16157–16162
72. Cockrell AS, Beall A, Yount B, Baric R (2017) Efficient reverse genetic systems for rapid genetic manipulation of emergent and pre-emergent infectious coronaviruses. Methods Mol Biol 1602:59–81
73. Menachery VD, Gralinski LE, Baric RS, Ferris MT (2015) New metrics for evaluating viral respiratory pathogenesis. PLoS One 10: e0131451